Toxicology in Vitro 24 (2010) 45–55

Contents lists available at ScienceDirect

Toxicology in Vitro

journal homepage: www.elsevier.com/locate/toxinvit

Oxidative stress, calcium homeostasis, and altered gene expression in human lung epithelial cells exposed to ZnO nanoparticles

Chuan-Chin Huang [a], Robert S. Aronstam [a,b], Da-Ren Chen [c], Yue-Wern Huang [a,b,d,*]

[a] Department of Biological Sciences, Missouri University of Science and Technology, 105 Schrenk Hall, 400 W. 11th Street, Rolla, MO 65409, United States
[b] Missouri S&T cDNA Resource Center, Missouri University of Science and Technology, 105 Schrenk Hall, 400 W. 11th Street, Rolla, MO 65409, United States
[c] Department of Energy, Environmental and Chemical Engineering, Washington University in St. Louis, Campus Box 1180, One Brookings Drive, St. Louis, MO 63130, United States
[d] Missouri S&T Environmental Research Center, Missouri University of Science and Technology, 105 Schrenk Hall, 400 W. 11th Street, Rolla, MO 65409, United States

ARTICLE INFO

Article history:
Received 18 April 2009
Accepted 10 September 2009
Available online 13 September 2009

Keywords:
Nanoparticles
ZnO
Oxidative stress
Calcium modulation
Cytotoxicity
Gene expression

ABSTRACT

The influence of 20 nm ZnO nanoparticles on cytotoxicity, oxidative stress, intracellular calcium homeostasis, and gene expression was studied in human bronchial epithelial cells (BEAS-2B). ZnO caused a concentration- and time-dependent cytotoxicity while elevating oxidative stress and causing membrane damage (cellular LDH release). There was a remarkably steep relationship between concentration and toxicity at concentrations from 5 to 10 μg/ml. Cytotoxicity was completely abolished by the antioxidant *N*-acetylcysteine (NAC). Exposure to ZnO also increased intracellular calcium levels ($[Ca^{2+}]_{in}$) in a concentration- and time-dependent manner that was partially attenuated by NAC. Nifedipine, a calcium channel blocker, partially attenuated the elevated $[Ca^{2+}]_{in}$, indicating that some of the excess $[Ca^{2+}]_{in}$ is a result of influx from outside the cell. The relationships between oxidative stress, $[Ca^{2+}]_{in}$, and cytotoxicity are discussed. Exposure to a sublethal concentration of ZnO increased the expression of four genes that are involved in apoptosis and oxidative stress responses BNIP, PRDX3, PRNP, and TXRND1, by at least 2.5-fold. Thus, ZnO alters transcriptional regulation in BEAS-2B cells.

1. Introduction

Nanomaterials have at least one dimension in the range of 1–100 nm. Due to their unique physical and chemical characteristics, nanomaterials have become widely used in the production of cosmetic products, transparent conductive films, and wave filters. Unintended exposure to nanomaterials may occur in occupational workers and end product users via inhalation, dermal absorption, or gastrointestinal tract absorption. Nanomaterials are thought to impose more serious adverse effects on organisms than microscale materials because of their smaller sizes and corresponding larger specific surface areas (Kipen and Laskin, 2005; Oberdorster et al., 2005; Nel et al., 2006). We and others have studied the adverse effects of nanomaterials with various compositions and properties on human health in *in vitro* and *in vivo* settings (Timblin et al., 2002; Li et al., 2003, 2006a,b, 2008, 2009; Möller et al., 2005; Jeng and Swanson, 2006).

Nanostructures of ZnO, including particles, rods, wires, belts, tubes, cages, walls, and rings, have attracted much attention due to their unique electronic and optoelectronic properties at nanoscale levels and their widespread application in catalysis, paints, wave filters, UV detectors, transparent conductive films, varistors, gas sensors, solar cells, sunscreens, and cosmetic products (Comini et al., 2002; Bai et al., 2003; Ramakrishna and Ghosh, 2003; Bae and Seo, 2004; Ding and Wang, 2004; Zhu et al., 2005; Huang et al., 2006). Inhalation of ZnO compromises pulmonary function in pigs and causes pulmonary impairment and metal fume fever in humans (Fine et al., 1997; Beckett et al., 2005). In our previous study, exposure of human bronchoalveolar carcinoma-derived cells (A549) to nano- and micro-size ZnO particles revealed much steeper dose-dependent cytotoxicity relationships than those seen with other metal oxides (Lin et al., 2009). Mechanistic studies suggest that the toxicity is due to elevated oxidative stress and oxidative DNA damage. In a dose- and time-dependent study by Xia et al., ZnO (13 nm) induced toxicity in BEAS-2B cell lines, leading to generation of reactive oxygen species, excitation of inflammation, and cell death (Xia et al., 2008).

In this study, we extended our previous studies to examine ZnO-mediated changes in cellular pathway-specific gene expression associated with oxidative stress and antioxidant defense in immortalized human bronchial epithelial cells (BEAS-2B). Further, the relationships between oxidative stress, intracellular calcium ($[Ca^{2+}]_{in}$) concentration, and cell viability were determined. The objectives of the present study were to understand the relationships between the following responses of BEAS-2B to ZnO

* Corresponding author. Address: Department of Biological Sciences, Missouri University of Science and Technology, 105 Schrenk Hall, 400 W. 11th Street, Rolla, MO 65409, United States. Tel.: +1 573 341 6589; fax: +1 573 341 4821.
E-mail address: huangy@mst.edu (Y.-W. Huang).

0887-2333/$ - see front matter © 2009 Elsevier Ltd. All rights reserved.
doi:10.1016/j.tiv.2009.09.007

nanoparticles: (1) cytotoxicity, (2) mechanism of cytotoxicity, (3) expression of oxidative stress responsive genes, and (4) intracellular calcium homeostasis.

2. Materials and methods

2.1. ZnO particles characterization

ZnO particles (20 ± 3.5 nm) at >99% purity were purchased from Nanostructured and Amorphous Materials (Los Alamos, New Mexico, USA). We characterized particle morphology, size, and agglomeration states using scanning electron microscopy (SEM) and transmission electron microscopy (TEM). Particle size analysis was carried out by measuring specific surface area (SSA, m^2/g) by the Brunauer, Emmett and Teler (BET) technique (Quantachrome; Nova 1000). X-ray diffractometry (XRD; Scintag 2000) was used to characterize particle crystallinity. These characterizations were performed in a dry state. Impurities in nanoparticles were measured using the inductively-coupled plasma-mass spectrometer (ICP-MS; Agilent ICP_MS 7500ce with SP-5 Autosampler) with routine elemental analysis setup. All samples were analyzed by dispersing the powders in a 1% HNO_3 solution.

ZnO nanoparticle suspensions were freshly prepared with medium immediately before each experiment. Suspensions were mixed vigorously, sonicated, and then immediately applied to BEAS-2B cells to minimize agglomeration. Hydrodynamic size (an indicator of agglomeration) of ZnO in BEAS-2B culture medium was characterized by a dynamic light scattering (DLC) method using a 100 μg/ml stock solution as well as a series of dilutions to 10 μg/ml.

2.2. Chemicals

Bronchial epithelial cell basal culture medium and supplemental growth factors were purchased from Lonza (Basel, Switzerland). Trypsin–EDTA (1×), ROS detection reagents, and Hank's balanced salt solution (HBSS) were obtained from Invitrogen (Carlsbad, CA, USA). *N*-acetylcysteine (NAC), penicillin–streptomycin, and Tris–HCl were purchased from Aldrich–Sigma (St. Louis, MO, USA). MTS assay kits were purchased from Promega (Madison, WI, USA). LDH assay kits were purchased from Takara (Takara Bio, Shiga, Japan).

2.3. Cell culture and treatment with ZnO particles

Immortalized human bronchial epithelial cells (BEAS-2B) were purchased from ATCC (Manassas, VA, USA). These continuously cultured cells are widely used as an *in vitro* model for studying the prevention of the development of human lung carcinomas, as well as for nanotoxicity testing (Prahalad et al., 2001; Park et al., 2008). The culture medium contained 500 ml BEBM basal culture medium, 0.5 ng/ml recombinant epidermal growth factor (EGF), 500 ng/ml hydrocortisone, 0.005 mg/ml insulin, 0.035 mg/ml bovine pituitary extract, 500 nM ethanolamine, 500 nM phosphoethanolamine, 0.01 mg/ml transferrin, 6.5 ng/ml 3,3′,5-triiodothyronine, 500 ng/ml epinephrine, 0.1 ng/ml retinoic acid, trace elements, and 5 ml of 10,000 unit/ml penicillin plus 10,000 μg/ml streptomycin.

Cells were grown at 37 °C in a 5% CO_2 humidified environment. To measure cytotoxicity (MTS), cell membrane damage (LDH) and intracellular oxidative stress levels (ROS), approximately 4000 cells were seeded into each well of a 96-well plate and allowed to attach and grow for 48 h before being treated. To measure gene expression, cells were seeded into 75 cm^2 flasks at a 30% confluence, and then allowed to attach and grow for 48 h. To reduce experimental variations and improve accuracy, ZnO particles were dried in a desiccator before being weighed on an analytical balance. A stock suspension of 100 μg/ml ZnO was prepared in cell culture medium and then various concentrations were achieved by dilution. Cells without ZnO particles served as controls in each experiment. Fresh medium without cells or nanoparticles was used as a blank in certain assays. In pilot studies, MTS and ROS assays performed using either 100 μl or 200 μl cell culture medium per well did not differ significantly. Accordingly, 100 μl of cell culture medium per well was used in subsequent experiments. A cell culture medium volume of 200 μl was used to provide sufficient volume for LDH detection.

2.4. Cytotoxicity and mechanism of ZnO nanoparticles in BEAS-2B cells

To determine the cytotoxicity of 20 nm ZnO, BEAS-2B cells were treated with 5, 6, 7, 8, 9, or 10 μg/ml of ZnO. Untreated cells served as a control group. Titanium dioxide (TiO_2) of 25 ± 3.4 nm (size range = 19.5–29.0 nm), which has been shown to cause 30% cell death in BEAS-2B cells at 20 μg/ml (Park et al., 2008), was included as a positive control. The MTS assay (Cell Titer 96® Aqueous One Solution Assay, Promega) was used to determine cytotoxicity. Absorbance was measured at 490 nm using a microplate reader (FLOURstat; BMG Labtechnonogies, Durham, NC, USA). A concentration-dependent cytotoxicity study was conducted with *N*-acetylcysteine (NAC) to identify a sublethal NAC level for subsequent determination of the mechanism of ZnO-induced toxicity. Potential detection interference between ZnO and the dye in MTS was taken into account in order to exclude false positives.

2.5. Intracellular ROS measurement

ROS generation was measured using 5-(and-6)-carboxy-2′,7′-dichlorodihydrofluorescein diacetate (carboxy-H_2DCFDA). A carboxy-H_2DCFDA stock solution of 10 mM (in ethanol) was diluted 500-fold in BEAS-2B culture medium to yield a 20 μM working solution. Cells were washed twice and then incubated with the H_2DCFDA working solution for 1 h in the dark (37 °C incubator). The cells were then washed twice with fresh medium, followed by exposure to 20 nm ZnO particles for 24 h. Fluorescence was then determined at 485 nm excitation and 520 nm emission wavelengths using a microplate reader.

2.6. LDH measurement

Release of lactate dehydrogenase (LDH) to the cell culture medium indicates cell membrane damage. LDH activity in the cell culture medium was determined using a LDH Kit (Takara Bio, Shiga, Japan). After ZnO exposure (with or without NAC), half the amount of the 200 μl cell culture medium was collected for LDH analysis. LDH catalyzes the conversion of NAD^+ to NADH. Thus, the rate of NAD^+ reduction is directly proportional to LDH activity. LDH activity is reported as percentage increase relative to control level. Absorption was measured at 490 nm.

2.7. Modulation of intracellular calcium concentrations ($[Ca^{2+}]_{in}$)

Fura-2 was used to measure intracellular calcium concentrations ($[Ca^{2+}]_{in}$). To study resting ($[Ca^{2+}]_{in}$ in cells exposed to ZnO, approximately 20,000 cells in 2 ml culture medium were seeded in a glass bottom culture dish (MatTek, Ashland, USA). Twenty-four hours later, the culture medium was discarded and the cells were treated for 6 h with 2 ml of new medium containing the desired ZnO concentration. To keep cells exposed to constant ZnO concentrations throughout the experiment, the following procedures were adopted. Forty minutes before terminating the experiment, 1.5 ml of the medium was removed, placed in a 2 ml tube, and

incubated at 37 °C. The remaining 0.5 ml of medium was removed, supplemented with 3.5 μl of 2 μM fura-2 AM, vortexed, and then added back to the cells. The cells were incubated for 20 min to allow efficient loading of membrane permeable fura-2 AM and cleavage of the acetoxymethyl group by intracellular esters to yield the Ca^{2+}-sensitive, membrane impermeable dye, fura-2. The entire medium was then removed and the cells were washed with fresh warm medium twice to eliminate extracellular fura-2 AM. Following this wash, the 1.5 ml of medium in the 2 ml tube was added back to the cells, which were then allowed to reach homeostasis by incubation for the remaining 20 min. The cells were then placed on the stage of an inverted fluorescence microscope (*InCyt Basic IM* Fluorescence Imaging System, Intracellular Imaging Inc.). The cells were excited at 340 nm and 380 nm while emission was monitored at 510 nm at an acquisition rate of 10 Hz. The ratio of fluorescence measured after excitation at the two wavelengths (F_{340}/F_{380}) was proportional to the free calcium concentration. In each independent experiment, 25 cells were selected to measure the $[Ca^{2+}]_{in}$ and averaged. The mean and standard deviation of the results from 3 separate experiments were determined. Exposure to 9 and 10 μg/ml ZnO for more than 6 h caused extensive cytotoxicity and cell detachment from the dish, preventing meaningful measurement. To investigate the role of ROS in $[Ca^{2+}]_{in}$ modulation, cells were co-treated with ZnO and the antioxidant NAC (0.1 mM).

2.8. Gene expression alteration by ZnO nanoparticles

A pathway-specific microarray comprised of probes for 84 oxidative stress and antioxidant defense relevant genes (Cat. no. PAHS-065, SuperArray Bioscience, Frederick, MD, USA) was used to investigate alterations in gene expression caused by exposure to ZnO nanoparticles in BEAS-2B cells. After treatment with a sublethal concentration of ZnO nanoparticles (5 μg/ml), approximately 6×10^6 cells were collected for RNA extraction using an RNeasy Mini Kit (Qiagen, Valencia, CA, USA). cDNA was reversed transcribed from the extracted RNA using a RT^2 First Strand Kit (SuperArray). cDNAs were then mixed with the RT^2 SYBR Green/Rox PCR master mix (SuperArray), and 40 polymerase chain reaction cycles were performed using a Mxp3000 Real-Time thermocycler (Stratagene, La Jolla, CA, USA). Five array replicates were performed. For quality assurance, human genomic DNA contamination (plate pos. no. H06), three reverse transcription controls (plate pos. nos. H07, H08, H09), and three positive PCR controls (plate pos. nos. H10, H11, H12) were included in each 96-well microarray plate. The housekeeping gene GAPDH (plate pos. no. H04) was used for normalization, and the data were analyzed with the $\Delta\Delta C_t$ method. The difference between the C_t values (ΔC_t) of the gene of interest and the housekeeping gene was calculated for each experimental sample. Then, the difference in the ΔC_t values between the experimental and control samples ($\Delta\Delta C_t$) was calculated. The fold-change in expression of the gene of interest between the two samples was equal to $2^{(-\Delta\Delta C_t)}$.

More detailed gene annotations, array layout, and gene tables regarding the array are available at http://www.sabiosciences.com/genetable.php?pcatn=PAHS-065A. Data analysis, manufacturer's performance data sensitivity, specificity, and reproducibility of the array are available at http://www.sabiosciences.com/rt_pcr_product/HTML/PAHS-065A.html#accessory.

2.9. Statistical analysis

In the toxicity studies, three independent experiments were conducted, using triplicates for each treatment group. Data are expressed as mean ± standard deviation. In this study, we are interested in between-group values; therefore, we used a one-tailed unpaired Student's *t* test. The *p* value was set at 0.05. In the microarray study, each treatment group contained five replicates. In correlation analysis, when all points were within the 0.95 bivariate normal ellipse, the two factors were significantly correlated at a 95% confidence level.

3. Results

3.1. ZnO particle characterization

Table 1 summarizes the physicochemical properties of ZnO particles. The size of primary ZnO particles measured by TEM was approximately 20 nm. The particle specific surface area measured by BET was 47.47 m^2/g. The equivalent BET diameter was 22.5 nm (assuming a density of 5.6 g/cm^3). X-ray diffraction (XRD) analysis revealed a zincite crystal structure (Fig. 1a). The estimated crystallite size was approximately 14 nm based upon the three biggest peaks in the XRD spectrum. A TEM image of ZnO particles is shown in Fig. 1b. The morphology of the particle cluster revealed by SEM is presented in Fig. 1c. Both images indicate that ZnO particles of 20 nm are highly agglomerated. The surface morphology of ZnO agglomerates is very random, and the surface condition is generally rough. When suspended in cell culture medium, the hydrodynamic sizes, an indication of ZnO nanoparticle agglomeration, ranged from 50 to 70 nm at ZnO concentrations between 5 and 50 μg/ml. At 100 μg/ml ZnO, the hydrodynamic size increased dramatically to 300 nm. The total purity of ZnO particle powder was greater than 97.9% (Table 2). The concentrations of elements such as Cu, Cr, Fe, V, and Co that may generate free radicals via the Fenton reaction were below detection limits (0.04 ppm).

3.2. ZnO cytotoxicity is dose- and time-dependent

There was a steep relationship between ZnO concentration and reduction in cell viability in BEAS-2B cells exposed to 20 nm ZnO particles (Fig. 2a). ZnO nanoparticle cytotoxicity was observed at concentrations as low as 5–6 μg/ml; there was a steep decline in cell viability at concentrations between 6 and 10 μg/ml. A time course study revealed that toxicity induced by 20 nm ZnO particles occurred within 6 h; toxicity was more pronounced after a 24 h exposure. ZnO nanoparticles did not interfere with any components of the MTS assay (data not shown).

3.3. ZnO particles induce oxidative stress and disrupt the integrity of cell membranes

Intracellular ROS levels were significantly increased after 6 h and 24 h exposure to all concentrations of ZnO examined (*p*'s <0.05; Fig. 2b). There was an inverse correlation between ROS

Table 1
Characterization of ZnO particles. Size distribution, equivalent BET diameter, specific surface area, crystallinity, and hydrodynamic size were determined by TEM, BET surface area analyzer, and X-ray diffraction (XRD).

Mean ± SD (size distribution)	Equivalent BET diameter (nm)	Specific surface area (m^2/g)	Crystallinity		Hydrodynamic size (nm)
			Structure	Size (nm)	
20 ± 3.5 nm (14.3–25.0 nm)	22.5	47.47	Zincite	14	50–300

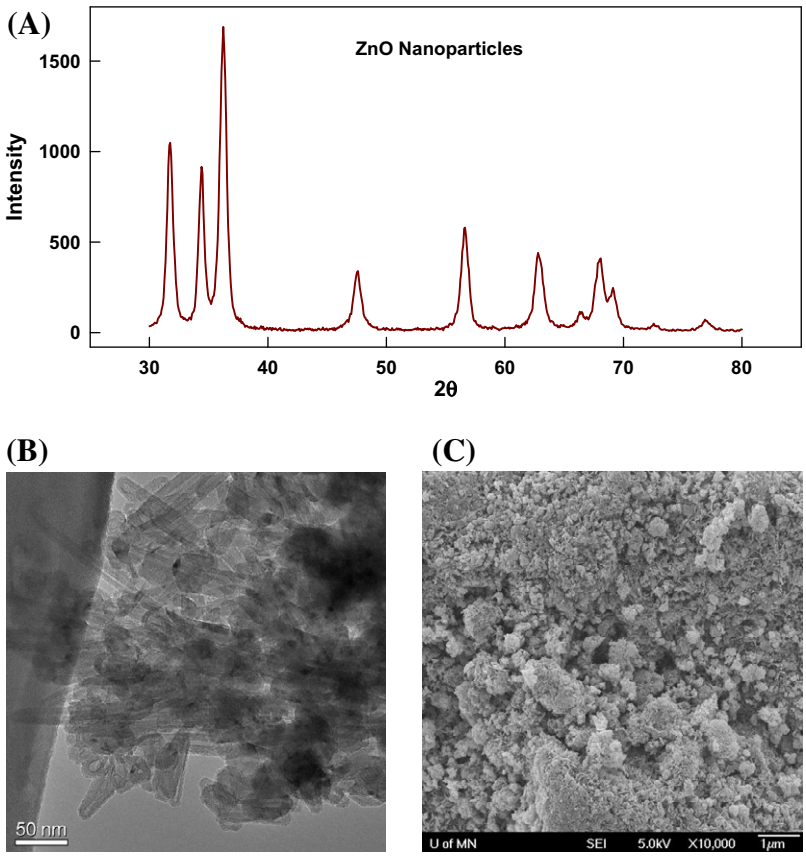

Fig. 1. (A) X-ray diffractometry, (B) transmission electron microscopy (TEM) and (C) scanning electron microscopy (SEM) of 20 nm ZnO particles.

Table 2
Metal impurity levels of ZnO particles in dry powder. Total purity is >97.9%. The detection limit of the inductively-coupled plasma-mass spectrometry (ICP-MS) system was 0.04 ppm.

Elements	Metal impurity (ppm)	Highest working conc. (μg/ml)
Sr	18,900	0.189
Cd	1700	0.017
Be, Fe, V, Mn, Co, Na, Mo, Cs, Ti, U, Na, K, Cu, Se, Ca, As, Pb, Mg, Ga, Al, Sb, Ti, Ni, Ag, Ba, Rb, Cr	Not detected	Not detected
Total	20,600	0.206

and cell viability (R^2 = 0.976; Fig. 2c) at 6 h. Cell membrane damage was reflected in LDH release from cells into the culture medium. LDH levels following 24 h exposure to ZnO at 5, 6, 7, 8, 9 and 10 μg/ml were increased by ~26%, 31%, 34%, 60%, 100% and 133%, respectively, compared to control cells (p's <0.05; Fig. 3a). The antioxidant NAC attenuated the elevation of LDH levels in cells exposed to ZnO (p's <0.05; Fig. 3b) There was a positive correlation between LDH activity and ROS level at both 24 h (R^2 = 0.953; Fig. 3c) and 6 h (data not shown).

3.4. N-acetylcysteine prevents cytotoxicity induced by ZnO particles

To further establish the role of oxidative stress in ZnO-induced cytotoxicity, cells were co-treated with an antioxidant, *N*-acetylcysteine (NAC). NAC was not toxic to BEAS-2B cells at concentrations below 1.0 mM (data not shown). Cotreatment of cells being exposed to 8 μf/ml ZnO with NAC increased cell viability by 88%, 90% and 92% at NAC concentrations of 0.1, 0.3 and 0.5 mM, respectively (Fig. 4). These results support the idea that oxidative stress causes the cytotoxicity, and suggests that NAC and other antioxidants may be effective in preventing or treating injuries resulting from exposure to ZnO nanoparticles.

3.5. ZnO alters the expression of certain genes involved in cellular responses to oxidative stress

The human oxidative stress and antioxidant defense PCR array that includes 84 OS-responsive genes was used to study ZnO effects on gene expression. The genes investigated are categorized as superoxide release and metabolism genes, peroxide metabolism genes, oxidoreductases genes, other genes involved in oxidative stress, inflammation related genes, apoptotic inducer genes, and cell cycle related genes. A sublethal, but ROS-elevating, concentration of ZnO (5 μg/ml) was used to avoid interference from disruption of intermediary metabolism, bioenergetics, and cell structure. Changes in gene expression in the ZnO-treated cells relative to control in a 24 h exposure paradigm are presented in Table 3. The expressions of BNIP3 (BCL2/adenovirus interacting protein 3), PRDX3 (peroxiredoxin 3), PRNP (Prion protein), and TRXND1 (thioredoxin reductase 1) were elevated by at least 2.5-fold above control levels (Fig. 5).

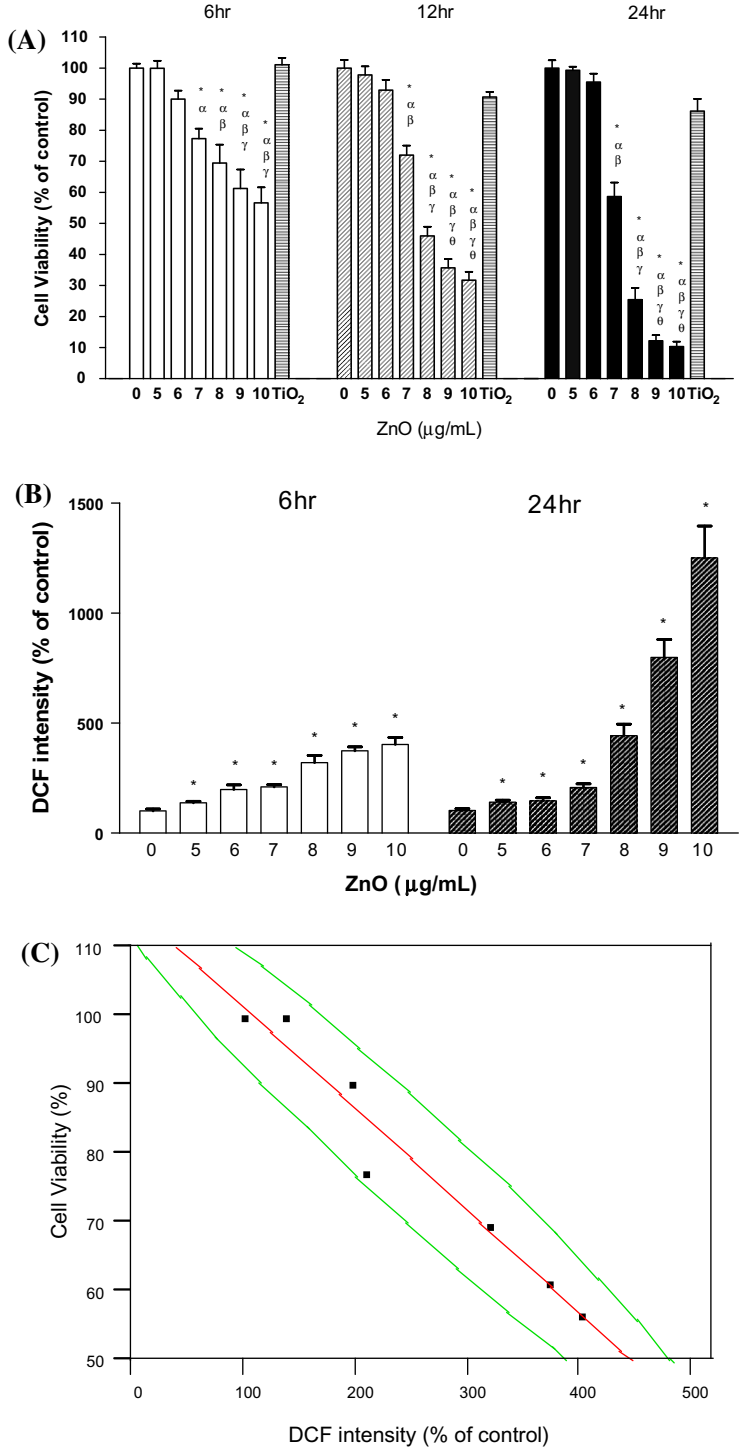

Fig. 2. (A) Time- and dosage-dependent cytotoxicity of 20 nm ZnO particles in BEAS-2B cells. Titanium dioxide (TiO_2) of 25 ± 3.4 nm (size range = 19.5–29.0 nm) at 20 μg/ml was used for comparison. Values are mean ± SD from three independent experiments performed in triplicate. (B) Oxidative stress induced by exposure of BEAS-2B cells to ZnO. After the cells were exposed to ZnO for 6 or 24 h, intracellular ROS levels were measured and normalized by the corresponding cell number. ZnO significantly elevated the intracellular ROS at all concentrations examined. (C) Inverse correlation ($R^2 = 0.976$) between intracellular ROS and viability of BEAS-2B cells exposed to ZnO for 6 h. Green lines indicate the bivariate normal ellipse $p = 0.950$. A 6 h exposure shows a similar pattern of correlation (data not shown). Significance is indicated by: $^{*}p < 0.05$ vs. control cells; $^{\alpha}p < 0.05$ vs. cells exposed to 5 μg/ml; $^{\beta}p < 0.05$ vs. cells exposed to 6 μg/ml; $^{\gamma}p < 0.05$ vs. cells exposed to 7 μg/ml; $^{\theta}p < 0.05$ vs. cells exposed to 8 μg/ml. (For interpretation of the references to colour in this figure legend, the reader is referred to the web version of this article.)

3.6. ZnO nanoparticles alter intracellular calcium levels in exposed cells

To understand the influence of oxidative stress on calcium homeostasis and to define the relationships between oxidative stress, calcium homeostasis, and cell viability, time- and dose-dependent measurements of intracellular calcium levels were performed. Dose dependent increases in $[Ca^{2+}]_{in}$ were observed in cells exposed to ZnO for 6 h (Fig. 6). At 9 and 10 μg/ml of ZnO, $[Ca^{2+}]_{in}$ increased to 330% and 370% of control levels, respectively. Increases of up to 2-fold were observed at 2 h and 3 h (data not shown). The antioxidant NAC partially attenuated these increases

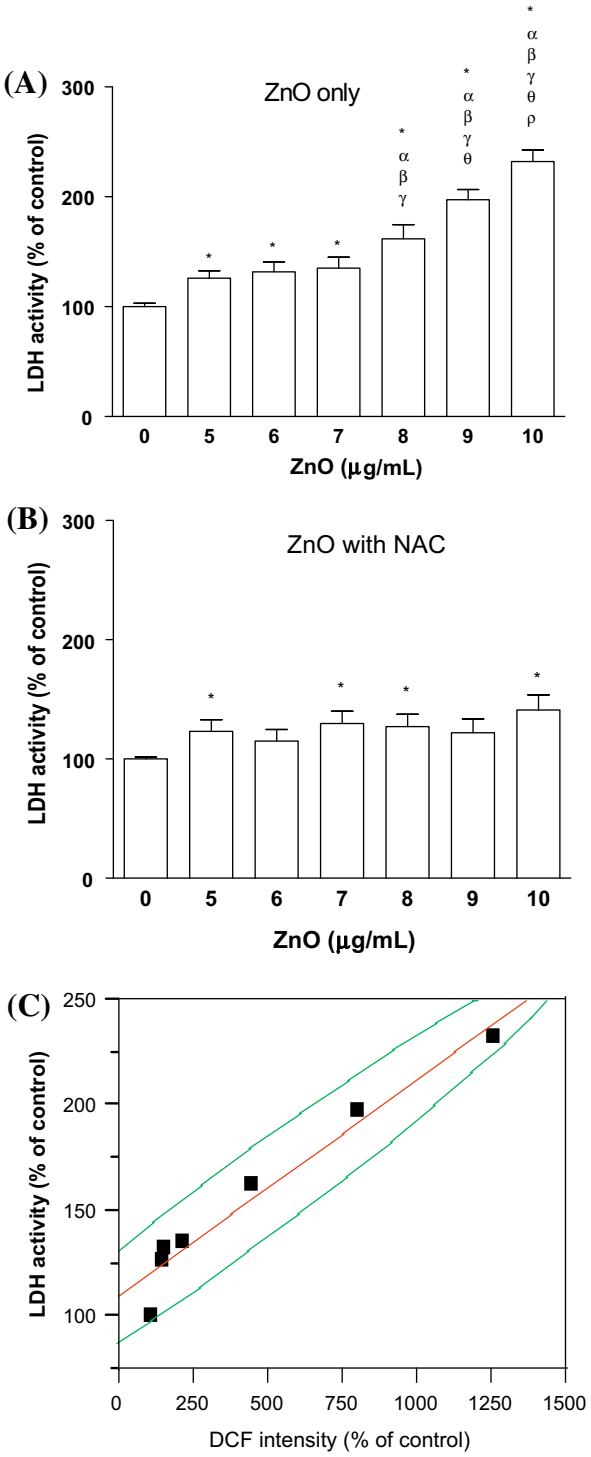

Fig. 3. LDH activities in the BEAS-2B cell culture medium following a 24 h exposure to ZnO only (A) or ZnO with NAC (B), respectively. The values are means ± SD from three independent experiments performed in triplicate. $^{*}p < 0.05$ vs. control cells; $^{\alpha}p < 0.05$ vs. cells exposed to 5 μg/ml; $^{\beta}p < 0.05$ vs. cells exposed to 6 μg/ml; $^{\gamma}p < 0.05$ vs. cells exposed to 7 μg/ml; $^{\theta}p < 0.05$ vs. cells exposed to 8 μg/ml; $^{\rho}p < 0.05$ vs. cells exposed to 9 μg/ml. (C) Positive correlation ($R^2 = 0.953$) between LDH activity (ZnO only) and ROS content of BEAS-2B cells exposed to ZnO for 24 h. A similar correlation at 6 h was observed after a 6 h exposure (data not shown). Green lines indicate the bivariate normal ellipse $p = 0.950$. (For interpretation of the references to colour in this figure legend, the reader is referred to the web version of this article.)

in $[Ca^{2+}]_{in}$ to levels 140% and 190% above control levels, respectively (Fig. 6a). Nifedipine, a calcium channel blocker, at a non-toxic level, diminished these increases in $[Ca^{2+}]_{in}$ to levels

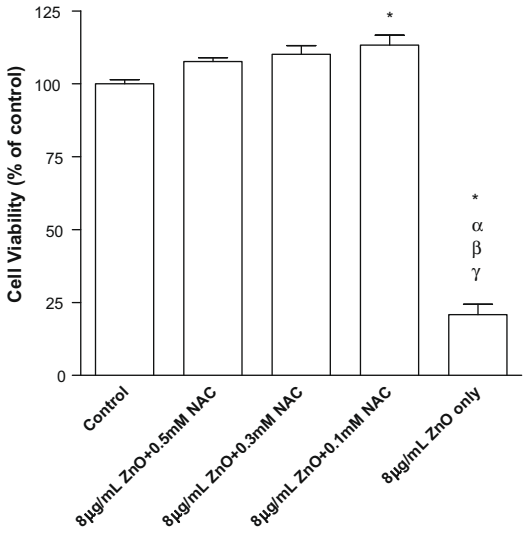

Fig. 4. The influence of the antioxidant *N*-acetylcysteine (NAC) on the reduction in cell viability caused by exposure to ZnO. Cells were incubated with 8 μg/ml ZnO with or without NAC for 24 h. Values are mean ± SD from three independent experiments each performed in triplicate. Significance: $^{*}p < 0.05$ vs. cells exposed to control cells; $^{\alpha}p < 0.05$ vs. cells exposed to 0.5 mM; $^{\beta}p < 0.05$ vs. cells exposed to 0.3 mM; $^{\gamma}p < 0.05$ vs. cells exposed to 0.1 mM.

150% and 200% above control levels (Fig. 6b). There was an inverse correlation between $[Ca^{2+}]_{in}$ and cell viability ($R^2 = 0.952$; Fig. 7).

4. Discussion

In a previous study we showed that exposure of A549 cells to 70 nm and 420 nm ZnO resulted in very steep dose–cytotoxicity curves spanning the range of 8–18 μg/ml (Lin et al., 2006a,b, 2008, 2009). These curves were steeper than those seen with other metal oxides particles, including Al_2O_3, TiO_2, and CeO_2. In this study, exposure of immortalized human bronchial epithelial cells (BEAS-2B) to 20 nm ZnO particles was studied. The immortalized cell line BEAS-2B provides a more suitable model for gene expression study than the cancer cell line A549. In these cells, ZnO also caused a steep cytotoxic response, with little toxicity being seen at 5 μg/ml and almost complete cell death at 10 μg/ml (24 h exposure). Thus, the steep dose–cytotoxicity phenomenon associated with ZnO particles is not cell line-dependent.

ZnO (20 ± 3.5 nm)-induced cytotoxicity was time-dependent; the toxicity developed within 6 h and was more pronounced after a 24 h exposure. Oxidative stress as reflected in ROS content and LDH release was elevated at all levels of ZnO concentrations, and this stress was positively correlated with the length of the exposure. The correlation of ROS, LDH, and cell viability suggest that elevated oxidative stress leads to cell death (Fig. 2c and 3c). It is worth noting that concentration specific analyses reveal that minor oxidative stress and cell membrane damage occur under exposure conditions (5 and 6 μg/ml, 6 and 24 h) that are insufficient to cause cytotoxicity.

Intracellular calcium concentration ($[Ca^{2+}]_{in}$) has major effects on cellular metabolism, signal transduction, and gene expression. $[Ca^{2+}]_{in}$ is tightly regulated, and increases in $[Ca^{2+}]_{in}$ are associated with cellular dysfunction, metabolic and energetic imbalance, disease states, and cell death. A host of environmental toxicants elevate $[Ca^{2+}]_{in}$ directly or indirectly by promoting Ca^{2+} influx, releasing Ca^{2+} from intracellular stores, inhibiting Ca^{2+} sequestration, or blocking Ca^{2+} efflux from the cell. In the present study, we determined the influence of acute exposure of ZnO nanoparticle on cytosolic calcium concentrations. ZnO did not change $[Ca^{2+}]_{in}$ in

Table 3
ZnO-mediated changes in cellular pathway-specific gene expression associated with oxidative stress and antioxidant defense in BEAS-2B cells.

Position	GeneBank	Gene Symbol	Description	Fold-change	Class*
A01	NM_000477	ALB	Albumin	0.65	4
A02	NM_000697	ALOX12	Arachidonate 12-lipoxygenase	1.09	1,3
A04	NM_001159	AOX1	Aldehyde oxidase 1	0.85	1
A05	NM_000041	APOE	Apolipoprotein E	0.67	4
A06	NM_004045	ATOX1	ATX1 antioxidant protein 1 homolog (yeast)	1.37	4
A07	NM_004052	BNIP3	BCL2/adenovirus E1B interacting protein 3	**3.59**	6
A08	NM_001752	CAT	Catalase	0.94	3
A09	NM_002985	CCL5	Chemokine (C–C motif) ligand 5	0.65	5
A10	NM_005125	CCS	Copper chaperone for superoxide dismutase	1.14	1
A11	NM_007158	CSDE1	Cold shock domain-containing E1, RNA-binding	1.12	4
A12	NM_000101	CYBA	Cytochrome b-245, alpha polypeptide	0.52	1
B01	NM_134268	CYGB	Cytoglobin	0.59	1
B02	NM_001013742	DGKK	Diacylglycerol kinase, kappa	0.64	4
B03	NM_014762	DHCR24	24-Dehydrocholesterol reductase	1.73	3, 6
B04	NM_175940	DUOX1	Dual oxidase 1	0.55	1, 2, 3
B05	NM_014080	DUOX2	Dual oxidase 2	0.68	1, 2, 3
B06	NM_004417	DUSP1	Dual specificity phosphatase 1	0.62	4, 7
B07	NM_001979	EPHX2	Epoxide hydrolase 2, cytoplasmic	0.62	3
B08	NM_000502	EPX	Eosinophil peroxidase	0.57	2
B09	NM_021953	FOXM1	Forkhead box M1	0.91	7
B10	NM_197962	GLRX2	Glutaredoxin 2	1.46	1, 6
B11	NM_153002	GPR156	G protein-coupled receptor 156	0.83	2, 3
B12	NM_000581	GPX1	Glutathione peroxidase 1	1.19	2, 3
C01	NM_002083	GPX2	Glutathione peroxidase 2	0.7	2, 3
C02	NM_002084	GPX3	Glutathione peroxidase 3	0.91	2, 3
C03	NM_002085	GPX4	Glutathione peroxidase 4	0.92	2, 3
C04	NM_001509	GPX5	Glutathione peroxidase 5	0.66	2, 3
C05	NM_182701	GPX6	Glutathione peroxidase 6	0.65	2, 3
C06	NM_015696	GPX7	Glutathione peroxidase 7	0.77	2, 3
C07	NM_000637	GSR	Glutathione reductase	1.45	2, 3
C08	NM_000178	GSS	Glutathione synthetase	0.91	4
C09	NM_001513	GSTZ1	Glutathione transferase zeta 1	0.92	2, 3
C10	NM_001518	GTF2I	General transcription factor II, i	0.75	1
C12	NM_006151	LPO	Lactoperoxidase	0.61	2, 3
D01	NM_000242	MBL2	Mannose-binding lectin (protein C) 2	0.59	5
D02	NM_004528	MGST3	Microsomal glutathione S-transferase 3	1.13	2
D03	NM_000250	MPO	Myeloperoxidase	0.62	2, 3
D04	NM_002437	MPV17	MpV17 mitochondrial inner membrane protein	1.16	1
D05	NM_012331	MSRA	Methionine sulfoxide reductase A	1.33	3
D06	NM_005954	MT3	Metallothionein 3	1.23	4
D07	NM_004923	MTL5	Metallothionein-like 5	1.07	4
D08	NM_000265	NCF1	Neutrophil cytosolic factor 1	0.55	1
D09	NM_000433	NCF2	Neutrophil cytosolic factor 2	0.59	1
D10	NM_003551	NME5	Non-metastatic cells 5	0.76	7
D11	NM_000625	NOS2A	Nitric oxide synthase 2A	0.62	3
D12	NM_024505	NOX5	NADPH oxidase	0.67	1
E01	NM_002452	NUDT1	Nudix-type motif 1	1	4
E02	NM_181354	OXR1	Oxidation resistance 1	0.88	4
E03	NM_005109	OXSR1	Oxidative-stress responsive 1	0.66	4
E04	NM_020992	PDLIM1	PDZ and LIM domain 1 (elfin)	1.14	4
E06	NM_007254	PNKP	Polynucleotide kinase 3'-phosphatase	0.5	4
E07	NM_002574	PRDX1	Peroxiredoxin 1	1.54	2, 3
E08	NM_005809	PRDX2	Peroxiredoxin 2	0.97	2, 3
E09	NM_006793	PRDX3	Peroxiredoxin 3	**13.36**	2, 3
E10	NM_006406	PRDX4	Peroxiredoxin 4	1.49	2, 3
E11	NM_181652	PRDX5	Peroxiredoxin 5	1.1	2, 3
E12	NM_004905	PRDX6	Peroxiredoxin 6	1	2, 3
F01	NM_020820	PREX1	PIP3-dependent RAC exchanger 1	0.72	1
F02	NM_006093	PRG3	Proteoglycan 3	0.64	4
F03	NM_183079	PRNP	Prion protein (p27-30)	**5.72**	4
F04	NM_000962	PTGS1	Prostaglandin-endoperoxide synthase 1	0.62	2
F05	NM_000963	PTGS2	Prostaglandin-endoperoxide synthase 2	0.59	2
F06	NM_012293	PXDN	Peroxidasin homolog (Drosophila)	0.99	2
F07	NM_144651	PXDNL	Peroxidasin homolog (Drosophila)-like	0.76	2
F08	NM_014245	RNF7	Ring finger protein 7	1.17	4
F09	NM_182826	SCARA3	Scavenger receptor class A, member 3	0.45	4
F10	NM_203472	SELS	Selenoprotein S	0.92	4
F11	NM_005410	SEPP1	Selenoprotein P, plasma, 1	0.96	4
F12	NM_003019	SFTPD	Pulmonary-associated protein D	0.74	1, 5
G01	NM_016276	SGK2	Serum/glucocorticoid regulated kinase 2	0.63	3, 7
G02	NM_012237	SIRT2	Sirtuin 2	0.64	4, 6
G03	NM_000454	SOD1	Superoxide dismutase 1	1.33	1, 3
G04	NM_000636	SOD2	Superoxide dismutase 2	0.89	1, 3

(*continued on next page*)

Table 3 (*continued*)

Position	GeneBank	Gene Symbol	Description	Fold-change	Class*
G05	NM_003102	SOD3	Superoxide dismutase 3	1.1	1, 3
G06	NM_080725	SRXN1	Sulfiredoxin 1 homolog (S. cerevisiae)	0.75	3, 4
G07	NM_006374	STK25	Serine/threonine kinase 25	0.52	4
G08	NM_000547	TPO	Thyroid peroxidase	0.72	2, 3
G09	NM_003319	TTN	Titin	0.72	2
G10	NM_032243	TXNDC2	Thioredoxin domain-containing 2	0.9	3
G11	NM_003330	TXNRD1	Thioredoxin reductase 1	**2.76**	3
G12	NM_006440	TXNRD2	Thioredoxin reductase 2	1	3

* 1 = Genes involved in superoxide release and metabolism; 2 = genes with peroxidase activity; 3 = genes with oxidoreductase activity; 4 = other genes involved in oxidative stress; 5 = inflammation relevant genes; 6 = apoptosis inducers; 7 = cell division relevant genes.

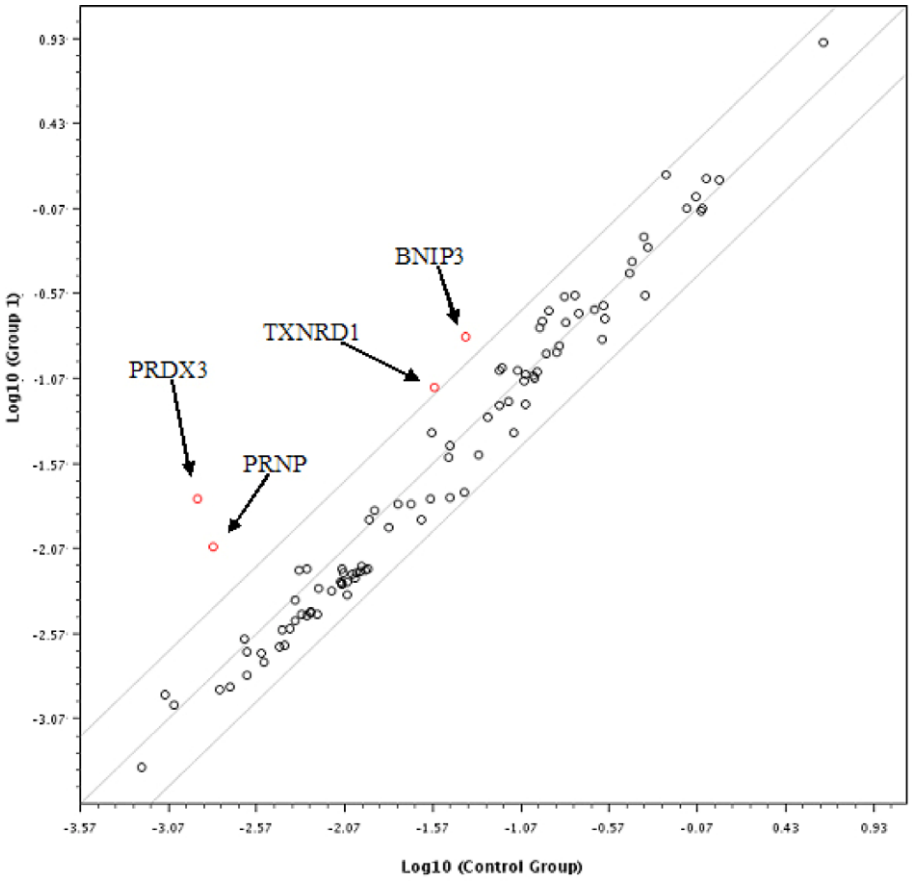

Fig. 5. Gene expression patterns in the BEAS-2B cells treated with 5 μg/ml 20 nm ZnO for 24 h. Red spots indicate the genes that were changed by at least 2.5-fold. (For interpretation of the references to colour in this figure legend, the reader is referred to the web version of this article.)

the first hour of exposure (data not shown). However, a 6-h exposure to ZnO caused a concentration-dependent elevation of $[Ca^{2+}]_{in}$, that was partially attenuated by the antioxidant NAC, indicating an effect of oxidative stress on calcium homeostasis. A shorter 2-h exposure to ZnO caused a 2-fold increase in $[Ca^{2+}]_{in}$ (data not shown). The inverse correlation between $[Ca^{2+}]_{in}$ and cell viability suggests a role for calcium in cell death. Reduction of $[Ca^{2+}]_{in}$ by NAC to levels approximately 50% higher than controls was sufficient to prevent cell death.

What, then, is the relationship between oxidative stress, calcium homeostasis, and cytotoxicity in nanotoxicity? ROS/RNS generation has been reported in response to inhaled particles, fibers, and nanomaterials (Mossman, 2003; Lin et al., 2006a,b). Stone et al. (2000) found that ROS were involved in the mechanism by which nanoparticles induce opening of plasma membrane Ca^{2+} channels in response to calcium release from the endoplasmic reticulum by thapsigargin. Studies using insults other than nanoparticles demonstrated that overproduction of ROS/RNS can be secondary to intracellular hypercalcaemia, as Ca^{2+} activates enzymes (e.g., hydrolytic enzymes, proteases, dehydrogenases in the citric cycle) that generate ROS/RNS (Nicotera et al., 1992; Leist and Nicotera, 1997; Harrison, 2002). ROS/RNS can oxidatively inactivate the thiol-dependent Ca^{2+} pump, which in turn aggravates the hypercalcaemia. Both ROS/RNS and hypercalcaemia can deplete cellular ATP reserves by multiple mechanisms. Severe primary metabolic disorders lead to ATP depletion, intracellular hypercalcaemia, ROS/RNS overproduction, and, thus, cell death (necrosis or apoptosis) (Szabo, 1996; Murphy, 1999; Dong et al., 2006; Giorgi et al., 2008).

Our findings are in agreement with this concept insofar as ZnO increases both ROS and intracellular Ca^{2+}. Moreover, there is an inverse correlation between ROS and cell viability (Fig. 2c), and

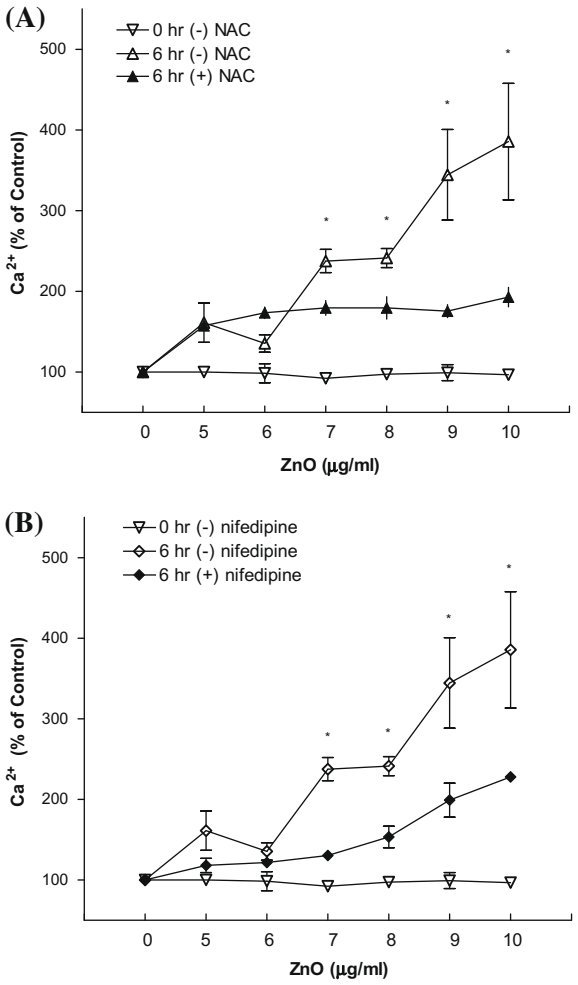

Fig. 6. Influence of ZnO nanoparticles, with or without NAC, on intracellular calcium concentrations. Intracellular calcium concentrations were measured immediately (0 h) or 6 h after ZnO exposure. Values are mean ± SD from three independent experiments each performed in triplicate; each replicate included separate measurements from 25 cells. $^{*}p < 0.05$ indicates statistical difference between 6 h (−) NAC and 6 h (+) NAC or between 6 h (−) nifedipine and 6 h (+) nifedipine.

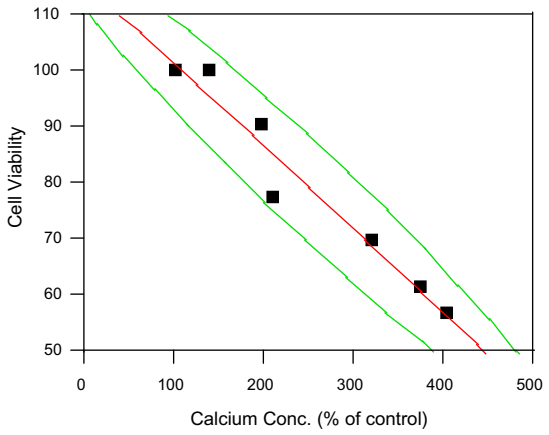

Fig. 7. The inverse relationship ($R^2 = 0.952$) between intracellular calcium levels and cell viability in ZnO-exposed BEAS-2B cells. The green lines indicate the bivariate normal ellipse $p = 0.950$. (For interpretation of the references to colour in this figure legend, the reader is referred to the web version of this article.)

the antioxidant NAC can prevent ZnO-induced cytotoxicity (Fig. 4). Our previous work (Lin et al., 2009) demonstrated OS-induced DNA strand breaks, supporting a connection between OS and cell death. Moreover, elevated $[Ca^{2+}]_{in}$ can be partially attenuated by antioxidant NAC (Fig. 6), and there is an inverse relation between $[Ca^{2+}]_{in}$ and cell viability (Fig. 7). Possible relationships among ROS, $[Ca^{2+}]_{in}$ and cell viability are summarized in Fig. 8.

Evidently, either ROS or calcium can initiate cytotoxic pathways in response to ZnO nanoparticles. ZnO may use its surface defect (redox active sites) to interact with unknown intracellular reductants to induce OS (and thereby affecting Ca^{2+} homeostasis). Alternately, ZnO may first interact with cytoplasm membrane causing loss of membrane integrity leading to calcium influx through membrane channels. Nifedipine partially attenuates the increase in $[Ca^{2+}]_{in}$, suggesting that a portion of the influx involves L-type calcium channels. Both intracellular calcium store release and plasma membrane damage due to lipid peroxidation may contribute to the influx of extracellular Ca^{2+} that cannot be suppressed by nifedipine. Additional studies are required to evaluate these possibilities.

A variety of cellular insults induce hypercalcaemia pathways that lead to cell death. In one nanoparticle study, Möller et al. (2005) demonstrated that calmodulin-dependent signaling pathways are crucial for cytotoxicity and cytoskeletal dysfunctions. The ZnO-induced calcium elevation observed in this study may cause cytotoxicity by similar or alternative mechanisms. Additional studies are required to identify the hypercalcaemia-mediated pathways that lead to cell death in the present model.

It is worth noting that NAC completely prevented cell death in response to ZnO while only partially attenuating the ZnO-induced increased in $[Ca^{2+}]_{in}$. Evidently, a doubling of $[Ca^{2+}]_{in}$ is not sufficient to cause cell death. Resistance to Ca^{2+} cytotoxicity has been reported by others (Weinberg et al., 1997; Dong et al., 1998).

One continuing issue in assessing nanotoxicity is agglomeration. Some recent studies suggest that bronchoalveolar lavage fluid (BALF) can de-agglomerate certain carbon black and titanium dioxide nanoparticles (Sager et al., 2007). Addition of BALF or surfactants may improve the suspension of nanoparticles in cell culture setting. It remains to be determined whether this treatment will influence studies on cellular signaling pathways and gene expression.

Since ZnO was observed to increase oxidative stress, we assessed the ability of ZnO to modulate the expression of stress responsive genes. In order to avoid interference from possible ZnO effects on intermediary metabolism, bioenergetics and cell structure, we selected a sublethal concentration of ZnO that reliably increases ROS. The expression of four genes was altered in the ZnO-treated cells. BNIP3 (BCL2/adenovirus E1B 19 kDa interacting protein 3) contains a BH3 domain and a trans-membrane domain that have been associated with pro-apoptotic activity. The dimeric mitochondrial protein encoded by this gene induces apoptosis (Wan et al., 2003). The up-regulation of the apoptotic inducer BNIP3 at a sublethal concentration of ZnO particles suggests that apoptosis directly reflects the cytotoxicity of ZnO nanoparticles. PRDX3 (peroxiredoxin 3), localized in the mitochondrion, belongs to the family of peroxiredoxin (Prx) enzymes that are thought to relieve cells from oxidative stress by removing the low levels of hydroperoxides produced during normal cellular metabolism (Jeong et al., 2006). PRNP (Prion protein) is important in regulating glutathione reductase activity (White et al., 1999). Because glutathione reductase functions in the regeneration of cellular GSH (glutathione), lower glutathione reductase activity would decrease the breakdown of oxidants by glutathione (Vassallo and Herms, 2003). TRXND1 (thioredoxin reductase 1) encodes a member of the family of pyridine nucleotide oxidoreductases that plays a role in selenium metabolism and protection against oxidative stress (Hintze et al., 2003). Thus, exposure of BEAS-2B

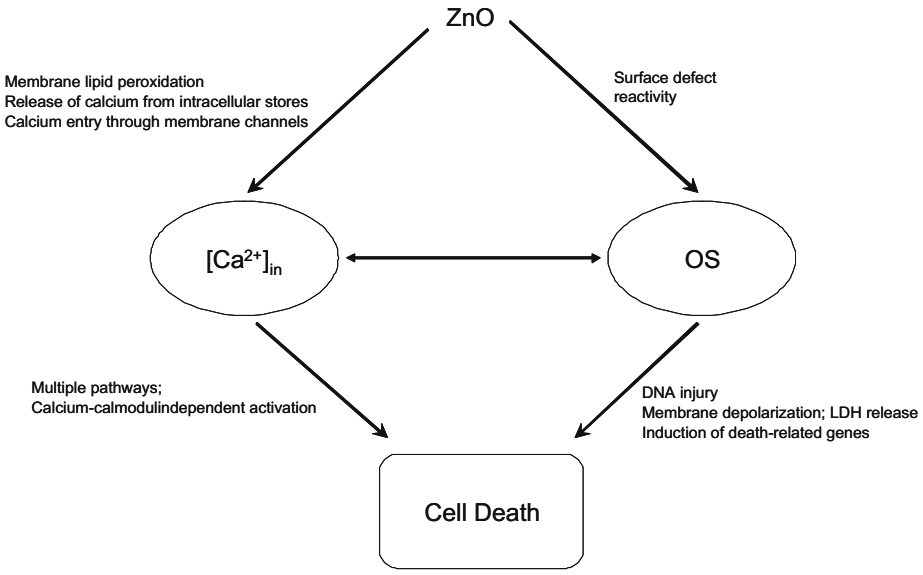

Fig. 8. Relationships between ZnO nanoparticles, production of reactive oxygen species (OS) and intracellular Ca^{2+} concentrations. The present results together with previous findings suggest that ZnO can trigger cell death by multiple pathways (Lin et al., 2008, 2009). ZnO increases $[Ca^{2+}]_{in}$ (present study, Stone et al., 2000). The moderation of this increase by nifedipine suggests that a portion of this increase reflects the influx of extracellular calcium; the possible involvement of Ca^{2+} release from intracellular stores has not been evaluated. Membrane disruption (e.g., by the demonstrated lipid peroxidation) may play a role in this influx. The increases in intracellular content OS may also have multiple sources. We postulate that the elevated OS is a consequence of ZnO surface defects interacting with intracellular reductants. Synergistic relationships between intracellular $[Ca^{2+}]$ and OS have been described (see text); in the present study, the ZnO increases in both were reduced by an antioxidant. Finally, while $[Ca^{2+}]_{in}$ and OS affect the activity of each other, they both induce cell death by distinct pathways.

cells to a sublethal concentration of ZnO nanoparticles induces the expression of at least four genes involved in oxidative stress and apoptosis. This is consistent with our biochemical and cytotoxicity findings. Surprisingly, the expression of several common antioxidant genes, including catalase, glutathione peroxidase, glutathione reductase, glutathione transferase, and superoxide dismutase, was not increased in cells exposed to ZnO. However, this finding is consistent with results obtained by Sarkar et al. (2007) with toxic single-walled carbon nanotubes in BJ Foreskin cells.

In summary, we have demonstrated that 20 nm ZnO particles induces cytotoxicity in cultured human bronchial epithelial cells (BEAS-2B) while elevating oxidative stress, cell membrane damage, and intracellular $[Ca^{2+}]_{in}$ in a concentration- and time-dependent fashion. Cytotoxicity can be completely abolished by the antioxidant NAC. The increase of $[Ca^{2+}]_{in}$ correlates with cytotoxicity and was partially reversed by treatment with NAC indicating connections between cytotoxicity, OS, and hypercalcaemia. Exposure to an OS-inducible, sublethal concentration of ZnO nanoparticles altered the expression of several genes that are involved in oxidative stress and apoptosis. Additional genetic analysis is required to appreciate the full nature and extent of this response.

Conflict of interest statement

None declared.

Acknowledgements

This work was supported by the Department of Biological Sciences and the cDNA Resource Center of the Missouri University of Science and Technology. The authors thank Yi Xu and Greg Schmoll for technical support.

References

Bae, S.Y., Seo, H.W., 2004. Vertically aligned sulfur-doped ZnO nanowires synthesized via chemical vapor deposition. Journal of Physical Chemistry 108, 5206–5210.

Bai, X.D., Gao, P.X., Wang, Z.L., Wang, E.G., 2003. Dual-mode mechanical resonance of individual ZnO nanobelts. Applied Physical Letter 28, 4806–4808.

Beckett, W.S., Chalupa, D.F., Pauly-Brown, A., Speers, D.M., Stewart, J.C., Frampton, M.W., Utell, M.J., Huang, L.S., Cox, C., Zareba, W., Oberdorster, G., 2005. Comparing inhaled ultrafine versus fine zinc oxide particles in healthy adults: a human inhalation study. American Journal of Respiration Critical care Medicine 171, 1129–1135.

Comini, E., Faglia, G., Sberveglieri, G., Pan, Z., Wang, Z.L., 2002. Stable and highly sensitive gas sensors based on semiconducting oxide nanobelts. Applied Physics Letter 81, 1869–1871.

Ding, Y., Wang, Z.L., 2004. Structure analysis of nanowires and nanobelts by transmission electron microscopy. Journal of Physical Chemistry 108, 12280–12291.

Dong, Z., Saikumar, P., Griess, G.A., Weinberg, J.M., Ventakachalam, M.A., 1998. Intracellular Ca^{2+} thresholds that determine survival or death of energy-deprived cells. American Journal of Pathology 152, 231–240.

Dong, Z., Saikumar, P., Weinberg, J.M., Venkatachalam, M.A., 2006. Calcium in cell injury and death. Annual Review of Pathology 1, 405–434.

Fine, J.M., Gordon, T., Chen, L.C., Kinney, P., Falcone, G., Beckett, W.S., 1997. Metal fume fever: characterization of clinical and plasma IL-6 responses in controlled human exposures to zinc oxide fume at and below the threshold limit value. Journal of Occupational and Environmental Medicine 39, 722–726.

Giorgi, C., Romaqnoli, A., Pinton, P., Rizzuto, R., 2008. Ca^{2+} signaling, mitochondria and cell death. Current Molecular Medicine 8, 119–130.

Harrison, R., 2002. Structure and function of xanthine oxidoreductase: Where are we now? Free Radical Biology and Medicine 33, 774–797.

Hintze, K.J., Wald, K.A., Zeng, H., Jeffery, E.H., Finley, J.W., 2003. Thioredoxin reductase in human hepatoma cells is transcriptionally regulated by sulforaphane and other electrophiles via an antioxidant response element. Journal of Nutrition 133, 2721–2727.

Huang, G.G., Wang, C.T., Tang, H.T., Huang, Y.S., Yang, J., 2006. ZnO nanoparticle-modified infrared internal reflection elements for selective detection of volatile organic compounds. Analytical Chemistry 78, 2397–2404.

Jeng, H.A., Swanson, J., 2006. Toxicity of metal oxide nanoparticles in mammalian cells. Journal of Environmental Science and Health, Part A Toxic/Hazardous Substances and Environmental Engineering 41, 2699–2711.

Jeong, W., Park, S.J., Chang, T.S., Lee, D.Y., Rhee, S.G., 2006. Molecular mechanism of the reduction of cysteine sulfinic acid of peroxiredoxin to cysteine by mammalian sulfiredoxin. Journal of Biological Chemistry 281, 14400–14407.

Kipen, H.M., Laskin, D.L., 2005. Smaller is not always better: nanotechnology yields nanotoxicology. American Journal of Physiology 289, L696–L697.

Leist, M., Nicotera, P., 1997. Calcium and neuronal death. Reviews of Physiology, Biochemistry and Pharmacology 132, 79–125.

Li, N., Sioutas, C., Cho, A., Schmitz, D., Misra, C., Sempf, J., Wang, M., Oberley, T., Froines, J., Nel, A., 2003. Ultrafine particulate pollutants induce oxidative stress and mitochondrial damage. Environmental Health Perspectives 111, 455–460.

Lin, W., Huang, Y.-W., Zhou, X.D., Ma, Y., 2006a. In vitro toxicity of silica nanoparticles in human lung cancer cells. Toxicology Applied Pharmacology. 217, 252–259. doi:10.1016/j.taap. 2006.10.004.

Lin, W., Huang, Y.-W., Zhou, X.D., Ma, Y., 2006b. Toxicity of cerium oxide nanoparticles in human lung cancer cells. International Journal of Toxicology 25, 451–457.

Lin, W., Isaac, S., Huang, Y.-W., Zhou, X.D., Ma, Y., 2008. Cytotoxicity and cell membrane depolarization induced by aluminum oxide nanoparticles in human lung epithelial cells A549. Toxicological and Environmental Chemistry 90, 983–996. doi:10.1080/02772240701802559.

Lin, W., Xu, Y., Huang, C.-C., Ma, Y., Shannon, K.B., Chen, D.-R., Huang, Y.-W., 2009. Toxicity of nano- and micro-sized ZnO particles in human lung epithelial cells. Journal of Nanoparticle Research 11, 25–39. doi:10.1007/s11051-008-9419-7.

Möller, W., Brown, D.M., Kreyling, W.G., Stone, V., 2005. Ultrafine particles cause cytoskeletal dysfunctions in macrophages: role of intracellular calcium. Particle and Fibre Toxicology 2, 7. doi:10.1186/1743-8977-2-7.

Mossman, B.T., 2003. Introduction to serial reviews on the role of reactive oxygen and nitrogen species (ROS/RNS) in lung injury and diseases. Free Radical Biology and Medicine 34, 1115–1116.

Murphy, M.P., 1999. Nitric oxide and cell death. Biochimica et Biophysica Acta 1411, 401–414.

Nel, A., Xia, T., Madler, L., Li, N., 2006. Toxic potential of materials at the nanolevel. Science 311, 622–627.

Nicotera, P., Bellomo, G., Orrenius, S., 1992. Calcium-mediated mechanisms in chemically induced cell death. Annual Review of Pharmacology and Toxicology 32, 449–470.

Oberdorster, G., Oberdorster, E., Oberdorster, J., 2005. Nanotoxicology: an emerging discipline evolving from studies of ultrafine particles. Environmental Health Perspectives 113, 823–839.

Park, E.J., Yi, J., Chung, K.H., Ryu, J.C., Park, K., 2008. Oxidative stress and apoptosis induced by titanium dioxide nanoparticles in cultured BEAS-2B cells. Toxicology Letters 180, 222–229.

Prahalad, A.K., Inmon, J., Dailey, L.A., Madden, M.C., Ghio, A.J., Gallagher, J.E., 2001. Air pollution particles mediated oxidative DNA base damage in a cell free system and in human airway epithelial cells in relation to particulate metal content and bioreactivity. Chemistry Research Toxicology 14, 879–887.

Ramakrishna, G., Ghosh, H.N., 2003. Effect of particle size on the reactivity of quantum size ZnO nanoparticles and charge-transfer dynamics with adsorbed catechols. Langmuir 19, 3006–3012.

Sager, T.M., Robinson, D.W., Victor, A., Lindsley, W.G., Schwegler-Berry, D.E., Castranova, V., 2007. Improved method to disperse nanoparticles for *in vitro* and *in vivo* investigation of toxicity. Nanotoxicology 1, 118–129.

Sarkar, S., Sharma, C., Yog, R., Periakaruppan, A., Jejelowo, O., Thomas, R., Barrera, E.V., Rice-Ficht, A.C., Wilson, B.L., Ramesh, G.T., 2007. Analysis of stress responsive genes induced by single-walled carbon nanotubes in BJ Foreskin cells. Journal of Nanoscience and Nanotechnology 7, 584–592.

Stone, V., Tuinman, M., Vamvakopoulos, J.E., Shaw, J., Brown, D., Petterson, S., Faux, S.P., Borm, P., MacNee, W., Michaelangeli, F., Donaldson, K., 2000. Increased calcium influx in a monocytic cell line on exposure to ultrafine carbon black. European Respiratory Journal 15, 297–303.

Szabo, C., 1996. DNA strand breakage and activation of poly-ADP ribosyltransferase: a cytotoxic pathway triggered by peroxynitrite. Free Radical Biology and Medicine 21, 855–869.

Timblin, C.R., Shukla, A., Berlanger, I., BeruBe, K.A., Churg, A., Mossman, B.T., 2002. Ultrafine airborne particles cause increases in protooncogene expression and proliferation in alveolar epithelial cells. Toxicology and Applied Pharmacology 179, 98–104.

Vassallo, N., Herms, J., 2003. Cellular prion protein function in copper homeostasis and redox signalling at the synapse. Journal of Neurochemistry 86, 538–544.

Wan, J., Martinvalet, D., Ji, X., Lois, C., Kaech, S.M., Von Andrian, U.H., Lieberman, J., Ahmed, R., Manjunath, N., 2003. The Bcl-2 family pro-apoptotic molecule, BNIP3 regulates activation-induced cell death of effector cytotoxic T lymphocytes. Immunology 110, 10–17.

Weinberg, J.M., Davis, J.A., Venkatachalam, M.A., 1997. Cytosolic-free calcium increases to grater than 100 micromolar in ATP-depleted proximal tubules. Journal of Clinical Investigation 100, 713–722.

White, A.R., Collins, S.J., Maher, F., Jobling, M.F., Stewart, L.R., Thyer, J.M., Beyreuther, K., Masters, C.L., Cappai, R., 1999. Prion protein-deficient neurons reveal lower glutathione reductase activity and increased susceptibility to hydrogen peroxide toxicity. American Journal of Pathology 155, 1723–1730.

Xia, T., Kovochich, M., Liong, M., Madler, L., Gilbert, B., Shi, H., Yeh, J.I., Zink, J.I., Nel, A.E., 2008. Comparison of the mechanism of toxicity of zinc oxide and cerium oxide nanoparticles based on dissolution and oxidative stress properties. ACS Nano 10, 2121–2134.

Zhu, B.L., Xie, C.S., Zeng, D.W., Song, W.L., Wang, A.H., 2005. Investigation of gas sensitivity of Sb-doped ZnO nanoparticles. Material Chemistry Physics 89, 148–153.